Mechanistic insights on nanosilica self-networking inducing ultra-toughness of rubber-modified polylactide-based materials

Jérémy Odent, Jean-Marie Raquez, Jean-Michel Thomassin, Jean-Michel Gloaguen, Franck Lauro, Christine Jérôme, Jean Marc Lefebvre, Philippe Dubois

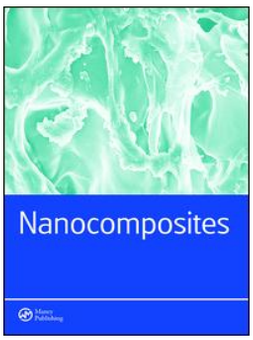

Nanocomposites

ISSN: 2055-0324 (Print) 2055-0332 (Online) Journal homepage: https://www.tandfonline.com/loi/ynan20

Mechanistic insights on nanosilica self-networking inducing ultra-toughness of rubber-modified polylactide-based materials

Jérémy Odent, Jean-Marie Raquez, Jean-Michel Thomassin, Jean-Michel Gloaguen, Franck Lauro, Christine Jérôme, Jean-Marc Lefebvre & Philippe Dubois

To cite this article: Jérémy Odent, Jean-Marie Raquez, Jean-Michel Thomassin, Jean-Michel Gloaguen, Franck Lauro, Christine Jérôme, Jean-Marc Lefebvre & Philippe Dubois (2015) Mechanistic insights on nanosilica self-networking inducing ultra-toughness of rubber-modified polylactide-based materials, Nanocomposites, 1:3, 113-125, DOI: 10.1179/2055033215Y.0000000005

To link to this article: https://doi.org/10.1179/2055033215Y.0000000005

Nanocomposites

Original Research Paper

Mechanistic insights on nanosilica self-networking inducing ultra-toughness of rubber-modified polylactide-based materials

Jérémy Odent[1], Jean-Marie Raquez[1]*, Jean-Michel Thomassin[2], Jean-Michel Gloaguen[3], Franck Lauro[4], Christine Jérôme[2], Jean-Marc Lefebvre[3] and Philippe Dubois[1]

[1]Laboratory of Polymeric and Composite Materials (LPCM), Center of Innovation and Research in Materials and Polymers (CIRMAP), University of Mons (UMONS), Place du Parc 20, B-7000 Mons, Belgium
[2]Center for Education and Research on Macromolecules (CERM), University of Liege, Sart-Tilman, Allée de la Chimie 3 B6, B-4000, Liege 1, Belgium
[3]Unité Matériaux et Transformations (UMET), UMR CNRS 8207, Université Lille1, Sciences et Technologies/CNRS, Cité Scientifique C6, 59655 Villeneuve d'Ascq, France
[4]Industrial and Human Automatic Control and Mechanical Engineering Laboratory (LAMIH), UMR CNRS 8201, University of Valenciennes and Hainaut-Cambresis, Le Mont Houy, BP 311, 59304 Valenciennes Cedex, France

Abstract Developing novel strategies to improve the impact strength of PLA-based materials is gaining a significant importance in order to enlarge the range of applications for this renewable polymer. Recently, the authors have designed ultra-tough polylactide (PLA)-based materials through co-addition of rubber-like poly(ε-caprolactone-*co*-D,L-lactide) (P[CL-*co*-LA]) impact modifier and silica nanoparticles (SiO_2) using extrusion techniques. The addition of silica nanoparticles into these immiscible PLA/P[CL-*co*-LA] blends altered their final morphology, changing it from rubbery spherical inclusions to almost oblong structures. A synergistic toughening effect of the combination of P[CL-*co*-LA] copolymer and silica nanoparticles on the resulting PLA-based materials therefore occurred. To explain this particular behavior, the present work hence aims at establishing the mechanistic features about the nanoparticle-induced impact enhancement in these immiscible PLA/impact modifier blends. Incorporation of silica nanoparticles of different surface treatments and sizes was thereby investigated by means of rheological, mechanical and morphological methods in order to highlight the key parameters responsible for the final impact performances of the as-produced PLA-based materials. Relying on video-controlled tensile testing experiments, a toughening mechanism was finally proposed to account for the impact behavior of resulting nanocomposites.

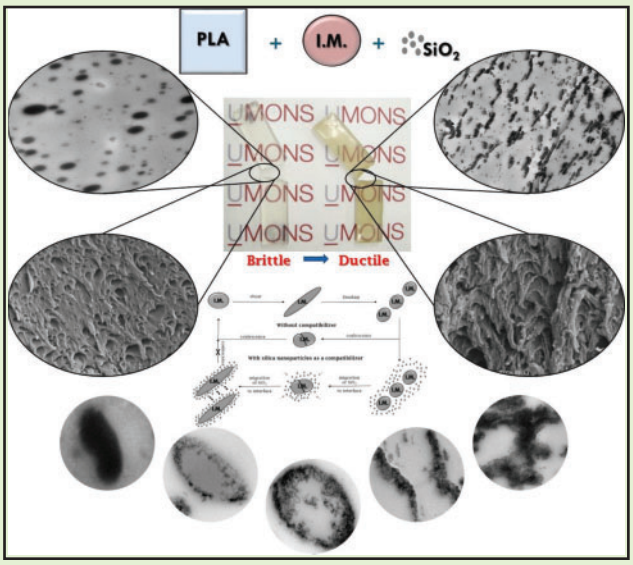

Keywords Polylactide, Impact modifier, Morphology, Compatibilization, Silica nanoparticles, Toughening mechanism

Cite this article Jérémy Odent, Jean-Marie Raquez, Jean-Michel Thomassin, Jean-Michel Gloaguen, Franck Lauro, Christine Jérôme, Jean-Marc Lefebvre and Philippe Dubois. *Nanocomposites*, 2015, 1, 113-125

Introduction

To generate rubber-toughened thermoplastics with optimal mechanical properties, the rubber phase morphology (domain size and related size distribution) and polymeric matrix–rubbery domain interfacial properties must be properly controlled.[1–5] The morphology of a two-phase system usually results to a balance between the breakup and coalescence of the dispersed domains in the flow field.[6] For uncompatibilized blends, the final particle size increases with the dispersed phase

*Corresponding author, email: jean-marie.raquez@umons.ac.be

Received 22 July 2014; accepted 24 February 2015
DOI 10.1179/2055033215Y.0000000005

concentration because of increased coalescence. Adding a compatibilizing agent to immiscible polymer blends enables to control the final morphology of these blends by lowering their interfacial tension,[7] resulting in a suppression, or at least, a decrease of coalescence extent in the dispersed phase.[8–10] Apart from reducing the interfacial tension, the role of a compatibilizer is to significantly enhance the adhesion between the continuous and dispersed phase within blend. Many authors reported different compatibilization routes through the utilization of organic compatibilizers like block or graft copolymers either preformed or generated *in situ* during flow-induced processes.[7,11–14] Recently, another compatibilization method has been reported through the addition of solid nanoparticles into immiscible polymer blends.[15–18] The role of the nanoparticles is to get specifically localized at the interface of both polymeric partners, to strengthen the interfacial adhesion between the partners and thus to enhance the overall material performances.[19–21] The use of nanoadditives (e.g. clay or silica nanoparticles) provides further advantages for polymeric blends such as enhanced material properties, ease of processing, and lower costs in comparison to block and graft copolymer compatibilizers.[22]

Ternary polymer composites containing glassy polymer, soft elastomer and rigid filler are also being the subject of an increasing number of studies.[23,24] The mechanical properties of such composites depend not only on the components but also on the phase structure (i.e. the relative arrangement of the components) and the phase size.[25] Concerning the phase morphology, separated microstructures where the elastomer and the filler are dispersed in the polymer matrix separately[26,27] and core–shell microstructures with the filler encapsulating the elastomer,[28,29] are the two current morphologies for these ternary composites. These distinct morphologies gave different mechanical performances with higher modulus and/or toughness in function of the dispersion extent.[30,31] Lipatov *et al.*[32–34] reported that the addition of solid particles into an immiscible polymer blend increases the thermodynamic stability of the mixture and changes the compositions of the separated phases. The authors proposed a simultaneous action of two mechanisms to explain the effect of fillers on the phase behavior: (i) the thermodynamical alterations at the interface because of the selective adsorption of one of both components and (ii) the redistribution of components at the interface and in the bulk that may diminish the phase-separation temperature.

The present contribution concerns ultra-tough immiscible polymer blends made of polylactide (PLA) rubber-toughened with poly(ε-caprolactone-*co*-D,L-lactide) (P[CL-*co*-LA]) copolyester and silica nanoparticles (SiO_2).PLA represents the most extensively investigated renewable polymer for substituting conventional petroleum-based polymers in different types of applications such as in automotive and electronic industries,[35,36] but suffers from its brittleness. This impedes its applications in some areas particularly like packaging materials.[37,38] Recently, the authors have reported the use of as-synthesized hydrolytically degradable P[CL-*co*-LA] copolymers as effective biodegradable impact modifiers for PLA.[39] Directly related to a control over the rubbery character of the dispersed phase and the morphological features of resulting blends, an optimum toughening effect was reached using a P[CL-*co*-LA] copolymer at a relative molar content of 28 mol%LA. The authors also reported that adding silica nanoparticles into these blends could alter their final morphology and then enhance the impact strength of these blends in such a way to achieve ultra-tough PLA-based materials.[40] As far as a toughening effect was evidenced, more understanding about the role of silica nanoparticles on the morphological features, the compatibility degree and the toughening mechanism of immiscible PLA/P[CL-*co*-LA] blends are however required to control the ultra-toughness of these blends. The authors here emphasize all issues aiming to clarify the morphology alteration for these immiscible PLA/P[CL-*co*-LA] blends through the use of silica nanoparticles of different surface treatments and particle size, leading to the construction of those silica nanoparticle-based self-networks. To achieve the best control over the blend morphology, it is well known that the final phase structure of ternary composites is governed by both thermodynamic (e.g. interfacial tension) and kinetic factors (e.g. shear stress and processing conditions).[19,41] In this respect, the authors have attempted to control the phase structure and the related-toughness of PLA/P[CL-*co*-LA]/SiO_2 composites upon coalescence and coarsening processes, i.e. by adjusting the nanoparticles dispersion and related processing methods used, and tuning the nanoparticle surface chemistry, mean size and relative content. Three types of silica nanoparticles, i.e. having different ability of self-agglomeration regarding surface treatment and surface area, and two processing methods (one-step or two-step) were mainly used to prepare the ternary composites for morphological, rheological and thermo-mechanical investigations. In addition, a special emphasis is made to highlight the toughening mechanisms related to the final mechanical performances of the as-produced PLA-based materials.

Experimental section

Materials

ε-caprolactone (99%, Acros) was dried for 48 h over calcium hydride and distilled under reduced pressure. D,L-lactide (> 99.5%, Purac) was conserved in a glove box. *n*-heptanol (98%, Aldrich) was dried over molecular sieve (4 Å) and tin(II) octoate ($Sn(Oct)_2$) (95%, Aldrich) was used as received without any purification, and diluted in dry toluene (0.01M). A commercially available extrusion-grade PLA (NatureWorks 4032D) designed especially for production of biaxially oriented films was used as received ($\overline{M_n}$ = 133 500 ± 5,000 g mol^{-1}, Đ = 1.94 ± 0.06 as determined by size-exclusion chromatography (SEC), 1.4 ± 0.2% D-isomer content as determined by the supplier). CAB-O-SIL TS-530 (TS-530, 225 m^2 g^{-1}) is of high surface area fumed silica, which has been surface modified with hexamethyldisilazane while CAB-O-SIL M-5 (M-5, 200 m^2 g^{-1}) and CAB-O-SIL H-5 (H-5, 300 m^2 g^{-1}) are untreated fumed silica and were supplied by Cabot.

Synthesis of poly(ε-caprolactone-*co*-D,L-lactide) copolymer

The copolymerization was carried out by bulk ring-opening polymerization (ROP) of ε-caprolactone and D,L-lactide promoted by *n*-heptanol and tin(II) octoate at an initial molar

[alcohol]/[tin(II) octoate] ratio of 100. The reaction was carried out for 24 h in an oil bath at 160°C, and quenched it in an ice bath. The crude product was dissolved in a minimum volume of chloroform, followed by precipitation into a 10-fold excess of heptane. They were recovered after filtration and drying under vacuum, until reaching a constant weight (yield: 99%).The LA molar content of the resulting copolymer was of 28 mol% (as determined by ^{1}H NMR analyses), while a number-average molecular weight of 35 400 g mol^{-1} (equivalent polystyrene) and a dispersity index (Đ) of 2.0 (as determined by GPC analyses) were achieved. This as-synthesized copolymer is amorphous with a glass transition temperature of about −36°C [as determined by differential scanning calorimetry (DSC) analyses].

Sample preparation and compounding

Before extrusion, PLA pellets were dried for at least 12 h at 80°C in an oven under reduced pressure of 10^{-1} mbar. Both binary and ternary PLA-based systems were prepared in a DSM twin-screw micro-compounder (15 cc) operated at 200°C and 60 rpm for 3 min. Two processing methods were employed to prepare PLA/P[CL-*co*-LA]/SiO_2ternary systems upon how these silica nanoparticles were dispersed, i.e. either directly into the blend (so-called one-step process) or first into one of the partners before blending (so-called two-step process) into PLA/P[CL-*co*-LA]-based systems. In the one-step process, both P[CL-*co*-LA] and silica were directly compounded with PLA, while in the two-step process silica nanoparticles were mixed first in one of the two partners by dissolving them in a minimal of chloroform. It was then followed by a slow evaporation of solvent under stirring and subsequently blended upon the same procedure as the one-step process. Standard samples of resulting PLA-based materials were then prepared by compression molding at 200°C for 10 min.

Characterization techniques

Proton nuclear magnetic resonance (^{1}H NMR) spectra were recorded in $CDCl_3$ using a Bruker AMX-500 apparatus at a frequency of 500 MHz. Size-exclusion chromatography was performed in THF (containing 2 wt-% NEt_3) at 35°C using a Agilent liquid chromatograph equipped with a Agilent G322A degasser, an isocratic HPLC pump G1310A (flowrate: 1 mL min^{-1}), a Agilent autosamplerG1329A (loop volume: 100 µL, solution concentration: 1 mg mL^{-1}),a Agilent-DRI refractive index detector G1362A and three columns: a guard column PLgel 10 µm and two columns PLgel mixed-B5 µm. Molecular weight and molecular weight distribution were calculated by reference to a relative calibration curve made of polystyrene standards. Differential scanning calorimetry was performed using a DSC Q2000 from TA Instruments at heating and cooling rates of 10°C min^{-1} under nitrogen flow (second scan). Notched Izod impact tests were performed according to ASTM D256 using a Ray-Ran 2500 pendulum impact tester (E = 4 J, mass = 0.668kg and speed = 0.46 m s^{-1}). Tensile tests were performed according to ASTM D638 using a Zwick universal tensile testing machine (speed = 1 mm min^{-1} and preload = 5 N). Dynamic mechanical thermal analyses (DMTAs) were performed under ambient atmosphere using a DMTA Q800 apparatus from TA Instruments in a dual cantilever mode. The measurements were carried out at a constant frequency of 1 Hz, a temperature range from −100°C to 150°C at a heating rate of 2°C min^{-1}. Data acquisition and analysis of the storage modulus (E'), loss modulus (E''), and loss tangent (tan δ) were recorded automatically. Rheological measurements were performed using a ARES Rheometer from Rheometrics. Frequency sweep measurements were recorded in linear regime conditions at a temperature of 200°C at a strain of 1%. Video-controlled mechanical testing was performed using an electro-mechanical machine Instron 5800 series. This equipment provides access to the true axial stress–strain curve, as well as to the local evolution of volume strain during the test. To ensure the localization of the plastic deformation at the center of the sample, a slight geometrical defect is machined out in the middle of the gage length of the dumbbell-shaped specimen (reduction about of 5% of the specimen width). Seven dot markers, made of dark ink, are printed on the front flat face of the sample (see Supplementary Material Fig. 1). Five of these dots are aligned and equally spaced in the tensile direction, x_3, while the two others are aligned with the central dot along the transverse direction, x_1.The axial true strain in the analysis zone, ε_3, is obtained by a polynomial interpolation of partial strains measured from the displacement of axial markers using Lagrange Transform and following Hencky's definition. For uniaxial tensile testing, the transverse strains, ε_1 and ε_2, are equal if the strain field is transversally isotropic in the center of the neck.[42–45] The volume strain, is simply computed from the trace of the true strain tensor: $\varepsilon_v = \varepsilon_1 + \varepsilon_2 + \varepsilon_3$. The volume strain can be positive, zero or negative. In particular, a volume increase is related to the occurrence of either crazing or cavitation (as in rubber-toughened blends), and in the opposite case, the authors consider that a compaction mechanism is active. Isovolumetric deformation mechanism refers to the activation of

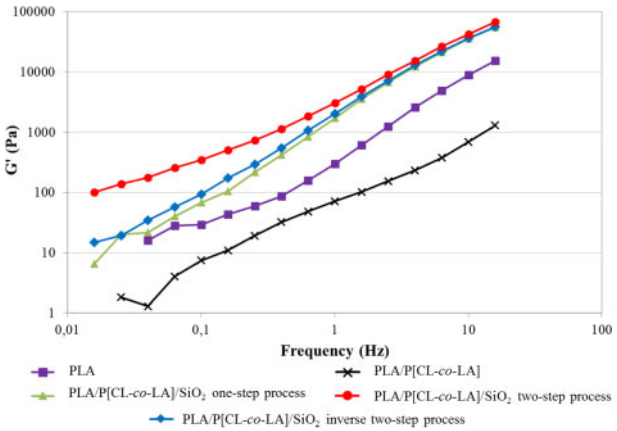

Figure 1 Rheological curves (storage modulus G' in function of frequency ν) of neat PLA (square, purple curve), PLA-based materials containing 10 wt-% P[CL-*co*-LA] (cross, dark curve) and corresponding blends containing 5 wt-% of silica nanoparticles (TS-530) produced via: one-step process (triangle, green curve), two-step process in which SiO_2 were first added into the P[CL-*co*-LA] partner (lozenge, blue curve) and two-step process in which SiO_2 were first added into the PLA partner (circle, red curve)

shear banding mechanisms (see Supplementary Material Appendix for more details). Room-temperature fractured surfaces of specimens were sputter-coated with gold and then examined through scanning electron microscopy (SEM) to highlight plastic deformation and possible toughening mechanisms. Accordingly, the room-temperature fracture was performed with a single column tensile test machine type Hounsfield H5KT with 5 kN cell force at a speed of 1 mm min^{-1} while SEM analyses were carried out using a Hitachi SU8020 (100 V–30 kV). Transmission electron microscopy (TEM) was carried out using a Philips CM20 microscope operated at 200 kV to investigate the morphological structure of resulting materials. To record TEM images, the samples were cryomicrotomed at −100°C by a Leica UCT microtome. Analysis software ImageJ was used for the analysis of TEM images to estimate the particle size and their distribution within the matrix.

Results

When P[CL-*co*-LA] copolymer and silica nanoparticles are used altogether, a simultaneous increase in toughness and stiffness in ternary PLA-based composites can be achieved in function of the processing method and the final blend morphology.[40] In this respect, a close relationship between mechanical performance and microstructure was first investigated on ternary PLA-based materials containing 10 wt-% of P[CL-*co*-LA] copolymer and 5 wt-% of TS-530 (225 $m^2 g^{-1}$, hexamethyldisilazane-modified SiO_2) upon how these silica nanoparticles were dispersed: either directly into the blend (so-called one-step process) or first into one of the polymeric partners (within PLA or P[CL-*co*-LA] partner) before blending with the second partner (so-called two-step process). Rheological investigations can be useful to monitor the formation of peculiar morphologies. Indeed, the rheological properties of the materials are strongly influenced by the extent of silica dispersion. It results to a significant increase of the storage modulus at low frequency when a physical network of (nano)particles is formed in the polymeric matrix (Fig. 1). It can be here observed that the storage modulus of PLA/P[CL-*co*-LA] blends containing 5 wt-% of TS-530 is only altered upon the aforementioned two-stage melt-process in which silica nanoparticles were first added into PLA. As a result, the two-stage melt-process gave access to the formation of a filler-network structure compared to the other methods.

To further explain this network, morphological investigations were carried out by TEM in order to highlight the blend morphology in function of the processing methods used (Fig. 2). In contrast to the one-step process and the two-step process in which SiO_2 were first added into the P[CL-*co*-LA] partner, it can be observed that almost oblong morphologies are achieved in the two-step process in which silica nanoparticles are first dispersed into the PLA partner (see see Fig. 2*d*). The achievement of such peculiar structures in which a physical network of silica nanoparticles is reached upon this selected processing method might ensure great overall material performances, implying the self-networking of silica nanoparticles at the PLA/P[CL-*co*-LA] interface.

As a result, toughness of resulting blends is definitely impacted by the way in which these nanoparticles were added (Table 1). Both one-step process (entry A) and reverse two-step process in which silica nanoparticles were first added into P[CL-*co*-LA] partner (entry B) show decreased toughness. In contrast, in the case of the two-stage melt-process, i.e. by first adding the silica nanoparticles into PLA matrix (entry C), a significant 10-times improvement of impact strength (as high as 27.3 kJ m^{-2} with 5 wt-% TS-530) and an increase of the materials elongation at break (closed to 42%) are recorded.

The effect of the surface treatment and surface area of silica nanoparticles at different contents was subsequently investigated on the morphology and properties of the PLA-based blends containing 10 wt-% of P[CL-*co*-LA] (Fig. 3). The aforementioned two-stage melt-process was in this regard considered, i.e. by adding first silica nanoparticles into PLA. Accordingly, TS-530 (225 $m^2 g^{-1}$, hexamethyldisilazane-modified SiO_2) and M-5 (200 $m^2 g^{-1}$, unmodified SiO_2) were selected as hydrophobic and hydrophilic silica nanoparticles of similar surface area respectively, while H-5 (300 $m^2 g^{-1}$, unmodified SiO_2) was selected as hydrophilic silica of higher surface area. From our TEM investigations, the major fraction of silica nanoparticles is aggregated around the P[CL-*co*-LA] dispersed phase as well as at the PLA/P[CL-*co*-LA] interface (e.g. *Figure* 3*a* and *b*). This so-implies the alteration of their final morphology, i.e. the conversion of regularly obtained spherical inclusions (as observed within PLA/P[CL-*co*-LA] binary blend, see Fig. 2*a*) into almost oblong structures in the presence of silica nanoparticles (e.g. *Figure* 3*c*). Surprisingly, whichever the silica nanoparticles considered, the as-formed oblong microdomains are interconnected at higher nanosilica content, leading to the formation of almost co-continuous morphologies (e.g. *Figure* 3*d*). Indeed, the junction of such peculiar oblong microstructures gradually appears at increasing nanoparticle content to reach an optimum at 10 wt-% TS-530, 5 wt-% M-5 and 3 wt-% H-5. However, it is worth noting that further increasing the nanoparticle content did not promote a larger extent of interconnection, but led to the main aggregation of silica nanoparticles within the blends more likely because of saturation of the PLA/P[CL-*co*-LA]interface.

Rheological measurements supports this statement, confirming the formation of interconnected structures (i.e. self-networked structures resulting from the migration of nanosilica into the PLA/P[CL-*co*-LA] interface) within PLA-based materials at these optimum contents of silica nanoparticles (Fig. 4). The large increase of the storage modulus in the lower frequency region again asserts the formation of filler-network structures, as indicated by the formation of a plateau in the low frequency regime.

As a result, the toughness of PLA-based materials is enhanced, up to 18 times, in the presence of silica nanoparticles within the PLA-based blends (Fig. 5) (see Supplementary Material Table 1 for tensile data). Indeed, synergistic toughening effects are obtained after the co-addition of P[CL-*co*-LA] copolymer and silica nanoparticles into PLA matrix, imparting enhanced toughness compared to PLA/SiO_2 (i.e. ≈3.5 kJ m^{-2}, 5 wt-%) and PLA/P[CL-*co*-LA] (i.e. 11.4 kJ m^{-2}, 10 wt-%) binary blends. For instance, the impact strength increases from

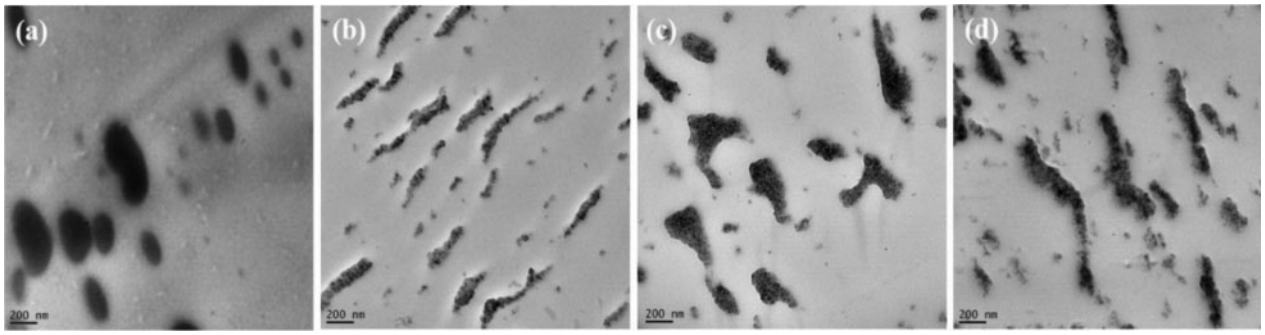

Figure 2 Transmission electron microscopy (TEM) micrographs (scale of 200 nm) of sample sections of PLA-based materials containing 10 wt-% of P[CL-*co*-LA] *a* and corresponding blends containing 5 wt-% of silica nanoparticles (TS-530) depending on the processing methods. Samples produced via: one-step process *b*, two-step process in which SiO_2 were first added into P[CL-*co*-LA] partner *c* and two-step process in which SiO_2 were first added into PLA partner *d*

Table 1 Influence of the processing method on the mechanical properties of PLA-based materials containing 10 wt-% of P[CL-*co*-LA] and 5 wt-% of silica nanoparticles (TS-530)

Entry	Processing methods	E^a/MPa	σ_y^a/MPa	ε_y^a/%	σ_b^a/MPa	ε_b^a/%	I.S.[b]/kJ m^{-2}
Ref. 1	PLA	1860 ± 40	–	–	58 ± 3	4 ± 0.5	2.7 ± 0.1
Ref. 2	PLA/P[CL-*co*-LA]	1680 ± 50	48 ± 3	4.0 ± 0.1	10 ± 0.5	21 ± 5	11.4 ± 0.3
A	One-step PLA/P[CL-*co*-LA]/SiO_2	1920 ± 54	52 ± 4	4.0 ± 0.2	11 ± 2	14 ± 4	7.9 ± 0.5
B	Two-step Pre-mix P[CL-*co*-LA]/SiO_2 + PLA	1920 ± 48	50 ± 1	4.0 ± 0.2	10 ± 0.2	16 ± 3	8.0 ± 0.4
C	Two-step Pre-mix PLA/SiO_2 + P[CL-*co*-LA]	1850 ± 53	47 ± 1	3.6 ± 0.1	13 ± 5	42 ± 16	27.3 ± 1.2

As determined by tensile tests at a drawing speed of 1 mm min^{-1} (ASTM D638). Young's modulus (E), yield stress (σ_y), yield strain (ε_y), fracture stress (σ_b) and strain at break (ε_b).
As determined by notched Izod impact tests (ASTM D256). Impact strength (I.S.).

2.7 kJ m^{-2} for the neat PLA up to 47.2 kJ m^{-2} upon the co-addition of 10 wt-% of P[CL-*co*-LA] and 5 wt-% of M-5. Interestingly enough, a maximum on the ultra-toughness implemented by the peculiar phase-morphologies was even recorded at 10 wt-% of TS-530 and 3 wt-% of H-5 (see Fig. 5). However, once higher loading of silica nanoparticles was used, actually higher than 10 wt-% of TS-530, 5 wt-% of M-5 or 3 wt-% of H-5, a drop in the toughness of resulting PLA-based blends occurs in relation to the presence of silica nanoparticle aggregates within the PLA-based blends (see Fig. 5).

As far as the extent of PLA crystallinity could largely improve impact toughness through a change in the deformation mechanism as crystallization occurs,[46] more investigations about thermo-mechanical features are also required in this work. In this respect and even if the crystallinity degree of PLA-based blends increased from 3 to 13% after adding 10 wt-% of P[CL-*co*-LA] copolymer within PLA, the DSC results did not show any major change on the thermal properties for the PLA/P[CL-*co*-LA] blends in the presence of silica nanoparticles (not reported here). In other terms, whichever the nanoparticles used and the silica content, the crystallinity of the blends remains in the same range of *ca.* 13–15%, highlighting no real relationship between thermal and impact properties of resulting blends. Dynamic mechanical thermal analysis was then used to explain this statement, measuring the thermodynamic response in flexion mode as a function of temperature for the neat PLA and immiscible PLA/P[CL-*co*-LA] blends upon the relative silica nanoparticles content (Fig. 6). While neat PLA is characterized by an apparent alpha transition (T_α) of about 61°C, two distinct peaks corresponding to both rubbery P[CL-*co*-LA] copolymer and PLA matrix are visible in the case of the binary blend at temperatures of −37°C and 59°C, respectively. Loading silica nanoparticles into these blends led to a shift of the characteristic T_α peak of P[CL-*co*-LA] to higher temperatures and the T_α peak of PLA toward lower temperatures (the difference of $\Delta T_{\tan\delta}$ was, respectively, about 5°C and 7°C at 5 wt-% and 10 wt-% TS-530), both in adequacy with an improved compatibility between the blend components (see Supplementary Material Fig. 2, for additional details).

To give access to the plastic response (i.e. elastic and non-elastic deformations) of resulting PLA-based materials in the presence or not of silica nanoparticles, a video-controlled mechanical testing method was used under uniaxial tension in this work (Figs. 7 and 8). Typical stress–strain curves are then noticed here, displaying very limited plastic deformation in neat PLA in contrast to large plasticity with a significant increase in ductility for the resulting rubber-toughened PLA-based blends (Fig. 7, top). This brittle-to-ductile transition is further supported by volume variation data analysis in which a dual response in terms of non-elastic deformation behavior was clearly recognized, i.e. the coexistence of dilatational (mechanisms inducing volume change such as cavitation, fibrillation and mainly crazing) (Fig. 7, middle) and non-dilatational (mechanisms inducing shearing without any volume change such as shear banding) (Fig. 7, bottom) mechanisms under sub-T_g drawing conditions.

In this respect, Fig. 8 reported the different contributions to the true strain, i.e. elastic strain, dilatational strain and shear strain within these PLA-based materials. As a result, the involved toughening mechanisms are mostly dilatational

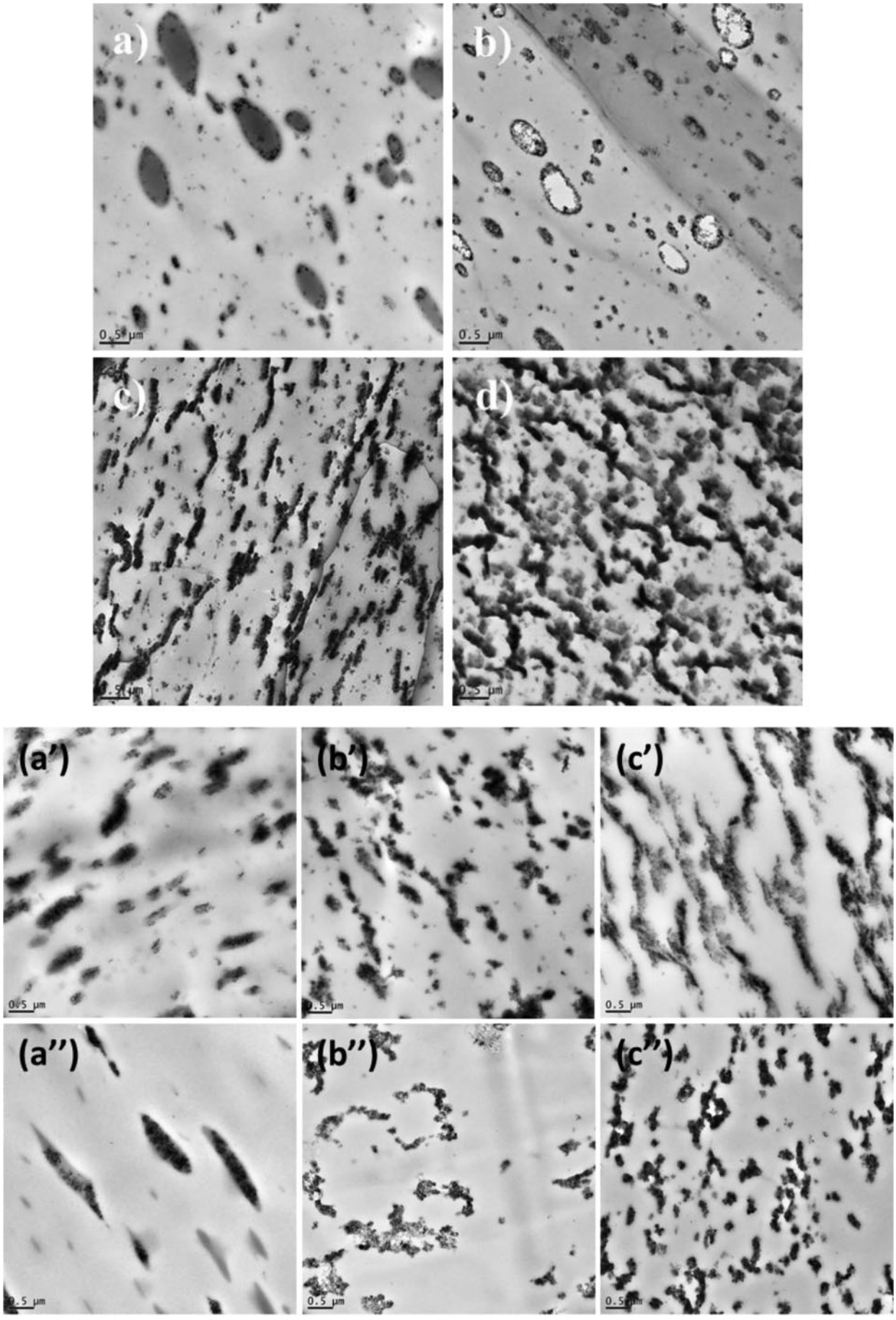

Figure 3 Transmission electron microscopy (TEM) micrographs (scale of 0.5 μm) of sample sections of PLA/P[CL-*co*-LA] blends containing TS-530 *a*, *b*, *c*, *d*, M-5 *a′*, *b′*, *c′* or H-5 *a″*, *b″*, *c″*: 1 wt-% *a*, *a′* and *a″*, 3 wt-% *b*, *b′* and *b″*, 5 wt-% *c*, *c′* and *c″* and 10 wt-% *d* of silica nanoparticles

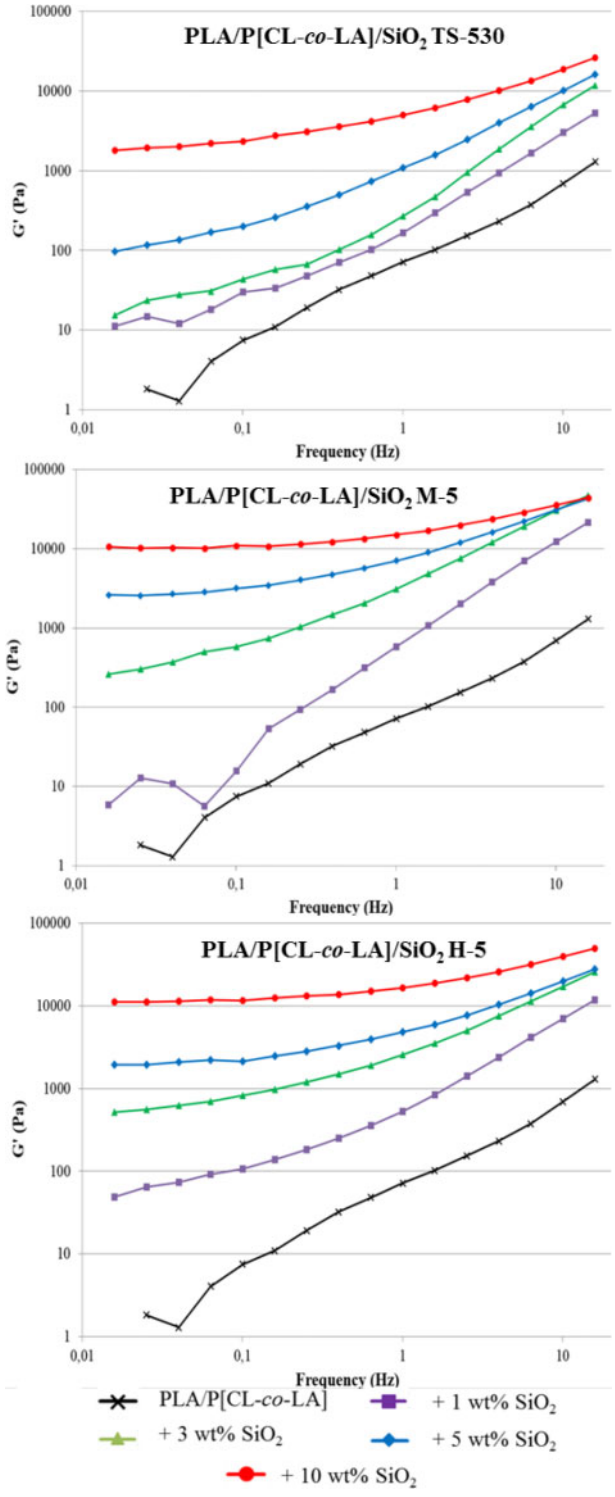

Figure 4 Rheological curves (storage modulus *G'* in function of frequency *ν*) of PLA-based materials containing 10 wt-% P[CL-*co*-LA] and TS-530 (top), M-5 (middle) or H-5 (bottom): 1 wt-% (square, purple curve), 3 wt-% (triangle, green curve), 5 wt-% (lozenge, blue curve) and 10 wt-% (circle, red curve) of silica nanoparticles in comparison with PLA/P[CL-*co*-LA] binary blend (cross, black curve)

in nature, i.e. the occurrence of crazing and/or cavitation and fibrillation appeared as the prevailing toughening mechanism for e.g. rubber-toughened PLA/P[CL-*co*-LA] binary blends (Fig. 8, top). As far as silica nanoparticles are loaded, greater energy dissipative micromechanisms are reached,

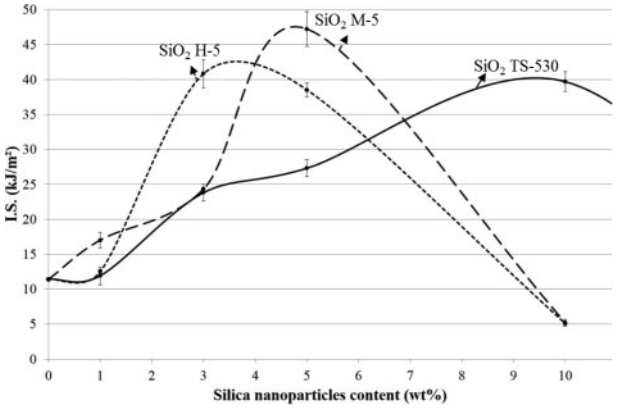

Figure 5 Dynamic mechanical thermal analysis (DMTA) thermograms (loss modulus in function of temperature) of unfilled PLA (green, solid line), PLA-based materials containing 10 wt-% of P[CL-co-LA] (dark, broken dash line) and corresponding blends filled with 5 wt-% (blue, long dash line) and 10 wt-% (red, short dash line) of silica nanoparticles (TS-530)

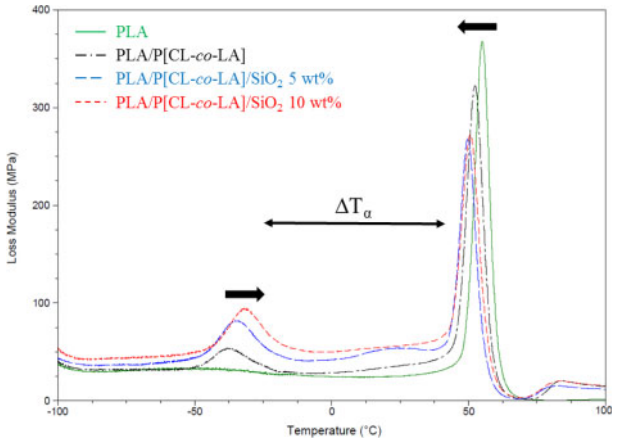

Figure 6 Notched Izod impact strength of PLA-based materials containing 10 wt-% of P[CL-*co*-LA] copolymer upon addition of silica nanoparticles: TS-530 (solid line), M-5 (long dash line) and H-5 (dash line)

i.e. enhanced cavitational modes (Fig. 7, middle) and the occurrence of shear banding (Fig. 7, bottom). In this respect, volume variation data analysis on PLA-based blends containing 5 wt-% of nanosilica clearly evidences that the early stage of plasticity is dominated by the occurrence of shear banding (Fig. 8, middle). Surprisingly, reaching the saturation of the PLA/P[CL-*co*-LA] interface in order to promote the formation of a filler-network and an interconnected structure obviously favored cavitational behavior at an early stage, which became more prominent than shear banding mechanism (Fig. 8, bottom).

High deformations and plasticity are furthermore evidenced on room-temperature fractured surfaces of these PLA-based materials (Fig. 9). As attested by SEM, macroscopic localized zones of micro-voids and micro-fibrils are found after addition of a rubbery P[CL-*co*-LA] impact modifier within the PLA matrix (Fig. 9, top). Surprisingly, the emergence of greater energy dissipative micromechanisms are further highlighted by loading silica nanoparticles within

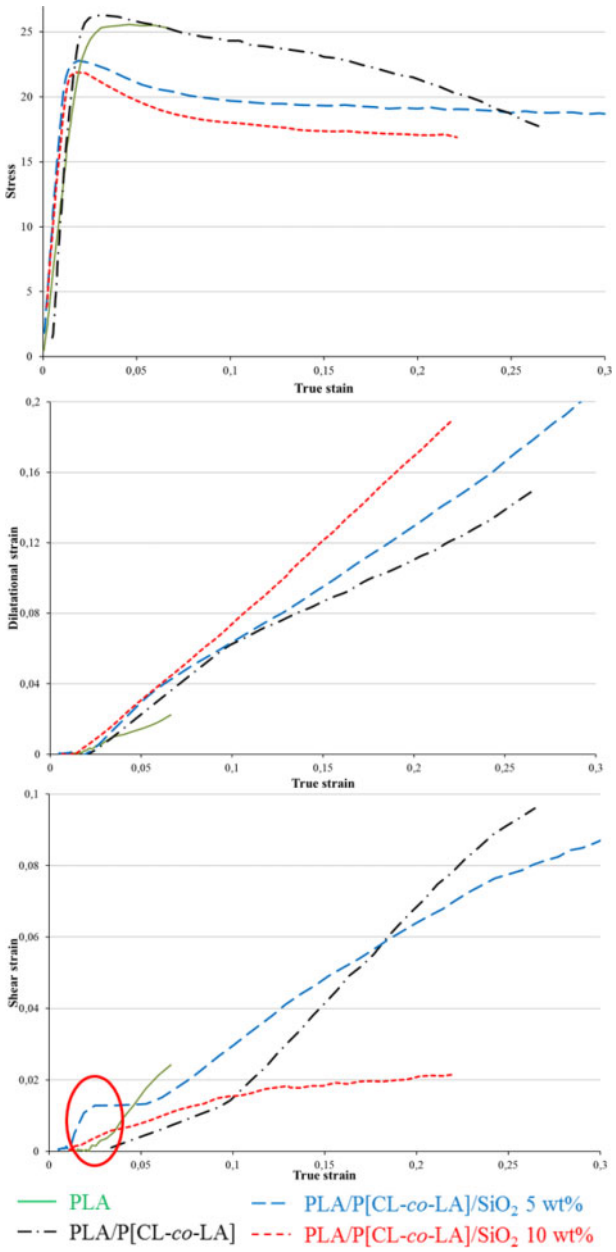

Figure 7 Typical stress-strain curves (top) and respective contributions of dilatational strain (middle) and shear strain (bottom) in unfilled PLA (green, solid line), PLA-based materials containing 10 wt-% of P[CL-*co*-LA] (dark, broken dash line) and corresponding blends filled with 5 wt-% (blue, long dash line) and 10 wt-% (red, short dash line) of silica nanoparticles (TS-530)

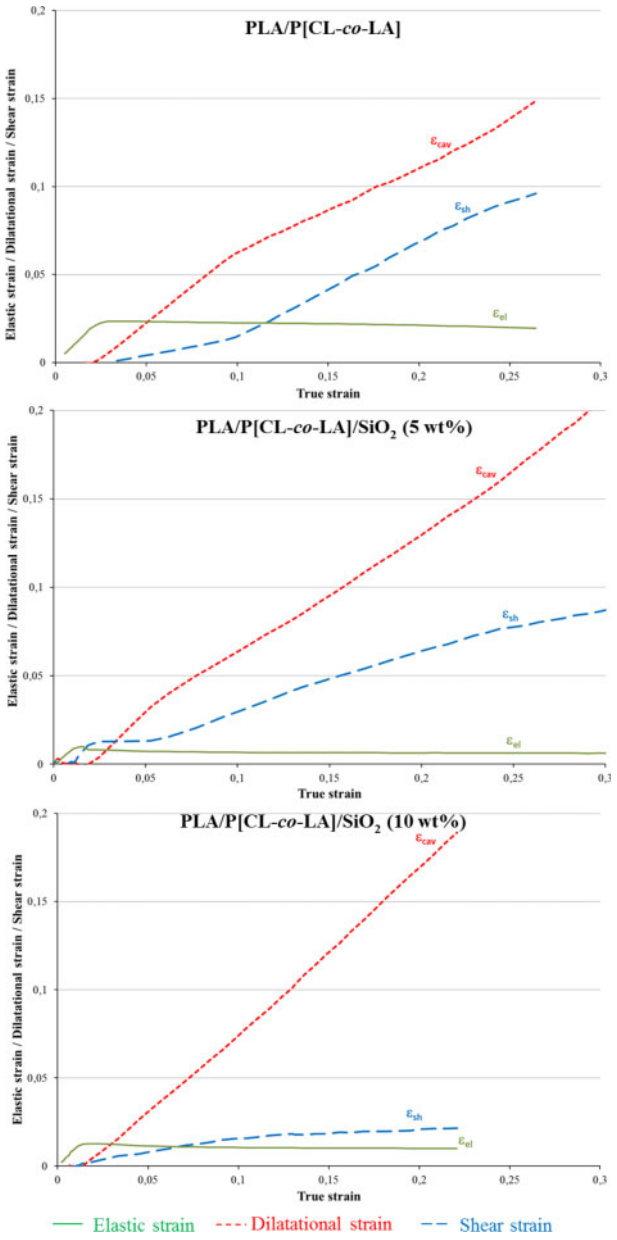

Figure 8 Contributions of elastic strain (ε_{el}, green, solid line), dilatational strain (ε_{cav}, red, short dash line) and shear strain (ε_{sh}, blue, long dash line) as a function of true strain in PLA-based materials containing 10 wt-% of P[CL-*co*-LA] (top) and corresponding blends filled with 5 wt-% (middle) and 10 wt-% (bottom) of silica nanoparticles (TS-530) as determined by video-controlled mechanical tests

these PLA/P[CL-*co*-LA]-based blends (Fig. 9, bottom). Indeed, SEM investigations reveal large-scale deformation and interpenetrating micro-fibrils within PLA/P[CL-*co*-LA]/SiO_2 ternary blends.

Discussions

For polymer systems, both thermodynamic (e.g. interfacial tension) and kinetic factors (e.g. shear stress and processing conditions) govern the final phase structure. This can explain how loading silica nanoparticles into the immiscible PLA/P[CL-*co*-LA] impact modifier blends may affect the morphological characteristic features. Indeed, thermodynamic factors are in favor of an embedded structure reducing the interfacial tension, while kinetic factors lead to a two-phase system independently of shear forces and viscosity of each polymeric partner. In this work, the kinetic contribution could be a prevailing parameter to explain why the silica nanoparticles can lead to these peculiar morphologies (i.e. oblong and even co-continuous structures), and therefore affect the overall performances of resulting nanocomposites. For instance, the reverse two-process strategy (where silica nanoparticles were first dispersed into the P[CL-*co*-LA] copolymer or the one-process strategy, rheological measurements indicate the absence of filler-network structure when 5 wt-% of TS-530 was used. In contrast and in the case of the

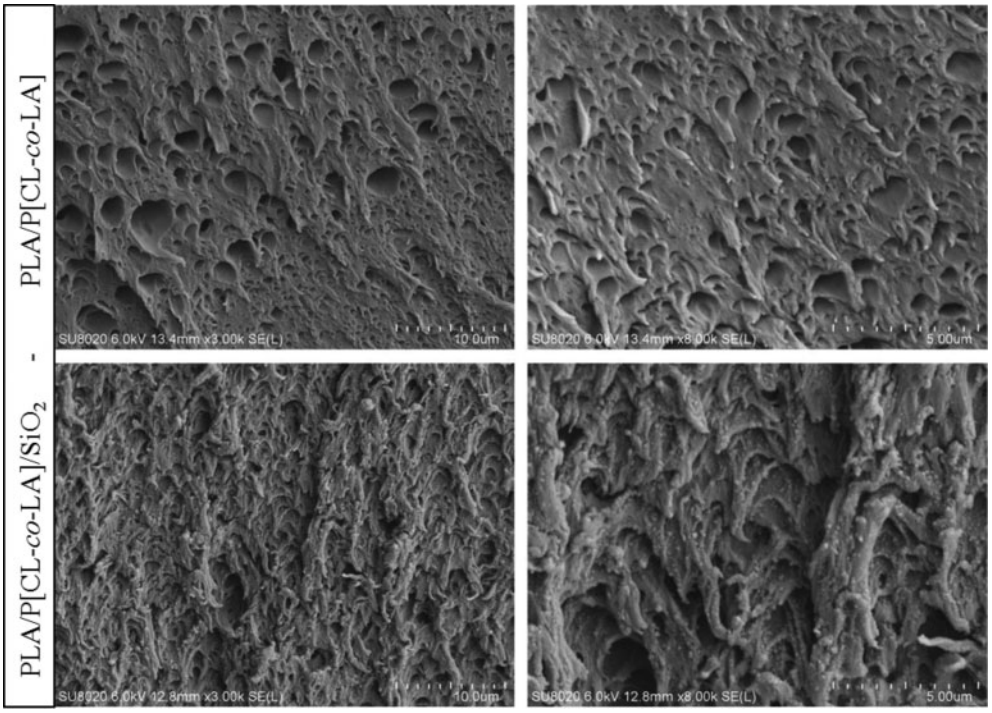

Figure 9 Scanning electron microscopy (SEM) micrographs (scale of 10 μm on left and zoom to 5 μm on right) of notched surfaces of PLA-based materials containing 10 wt-% of P[CL-*co*-LA] (top) and corresponding blend filled with 5 wt-% of silica nanoparticles (TS-530) (bottom)

two-process strategy in which silica nanoparticles were first dispersed into the PLA partner, the formation of filler-network structures (as previously evidenced by rheology, Figs. 1 and 4) can be noticed and be explained by the fact that the silica nanoparticles were mainly located in the PLA phase and could readily migrate toward the interface of the blends on processing. As a result, oblong structures are here obtained as evidenced by TEM measurements (Figs. 2 and 3). Similar trend was already reported by Yang *et al.*[19] highlighting the dependence of the phase morphology and the formation of the filler-network structure upon interfacial interactions in relation to the migration of silica to the interface. However, it could not be excluded that these silica nanoparticles can affect the overall viscosity of these blends and therefore can control the migration extent of silica nanoparticles within these blends as an additional feature.

From a thermodynamic viewpoint, wetting coefficient and interfacial tension are among the main parameters that can also affect the preferential affinity between the particles and polymeric phases. Such a behavior has been reported after addition of nanoparticles into immiscible polymer blends as an effective method to compatibilize the resulting blend, owing to their migration and localization at the blend interface used in these works.[15–21] However, Lipatov *et al.*[32–34] highlighted that the effect of filler introduction is mostly based on the thermodynamics of interaction near the surface. In this work, the silica nanoparticles do not have any specific affinity with respect to both polymeric partners, and tend to readily migrate at the PLA/P[CL-*co*-LA] interface where the interfacial adhesion is the lowest. If considered, the selective location of nanoparticles could be merely affected upon the hydrophilic–hydrophobic balance (and then the nanoparticles surface treatment). As a result, different optimum contents for these silica nanoparticles are reached upon their ability to self-agglomerate them at the interface upon their non-affinity towards both polymeric partners (PLA and P[CL-*co*-LA]). Accordingly, these different types of silica nanoparticles can be classified as follows: TS-530 < M-5 < H-5. A possible explanation to support this classification may arise from the preferential wetting between silica nanoparticles and P[CL-*co*-LA] phase upon both surface treatment and size of silica nanoparticles, resulting in the migration of the major fraction of silica nanoparticles at the PLA/P[CL-*co*-LA] interface. For instance, related to the facilitated motion of these silica nanoparticles to migrate to the interface as a function of their particle size, hydrophilic (without any surface treatment) silica nanoparticles of smaller particle size (higher surface area) can easily migrate from PLA matrix phase to the P[CL-*co*-LA] dispersed phase and their interface. In other terms, the lowest optimum content is achieved when hydrophilic silica nanoparticles (H-5) are used by decreasing their interfacial adhesion more significantly than others.

The morphological characteristic features, a key-parameter of this study, may explain how the nanoparticles in function of their surface treatment and surface area can strongly control ultra-toughness of these blends (Fig. 5 as a reminder). It is well known that the overall shape, average dimensions and related size distribution of the dispersed rubbery phase must be properly controlled to reach the compositions with optimal mechanical properties. From this work, the highest alteration in the blend morphology is guided by the extent of migration of silica nanoparticles into the PLA/P[CL-*co*-LA] interface. Zhang *et al.*[47] reported similar trends within immiscible polypropylene/polystyrene blends, showing a drastic reduction of polystyrene phase-size and a very

homogeneous size distribution through the addition of silica nanoparticles. This owes to the role of silica nanoparticles acting as interfacial compatibilizer and allowing enhanced compatibility degree and lower interfacial tension between both immiscible partners (as previously evidenced by DMTA, Fig. 6).This therefore induces the self-networking of silica nanoparticles at the interface and leads to the formation of these peculiar structures (see Fig. 3). As a result, the as-modified interfacial adhesion between polymeric partners upon the addition of silica nanoparticles led to a marked improvement of fracture-resistance for the resulting blends through these peculiar energy dissipative structures. At this stage, it can be claimed out that the resulting `infinite' network made of elongated rubbery domains affords a more efficient toughening scheme, as compared to the individually dispersed spherical microdomains.

Regarding the mechanism involved, the addition of silica nanoparticles to the immiscible PLA/P[CL-*co*-LA] blend influences the coalescence and breakup of the rubbery droplets and causes the shape and average size of the dispersed microdomains depending on the location of nanosilica (Scheme 1). For uncompatibilized blends such as PLA/P[CL-*co*-LA] blends, the morphology evolution is derived from the formation of large droplets of the dispersed rubbery P[CL-*co*-LA] phase within the PLA matrix in the molten state and the deformation of P[CL-*co*-LA] droplets under the shear force. During processing, the breakup of the dispersed/deformed P[CL-*co*-LA] phase into smaller microdomains is followed by a coalescent process. However, the system tends to minimize its total free energy and loading silica nanoparticles within this PLA/P[CL-*co*-LA] blend results in the migration of nanosilica into the phase for which they exhibit the stronger affinity and the lower interfacial tension, i.e. mainly at the PLA/P[CL-*co*-LA] interface. The nanoparticle selective location at the PLA/P[CL-*co*-LA] interface stabilizes the polymer phase morphology by decreasing the interfacial interaction, while the nanosilica migration and their self-networking among the P[CL-*co*-LA] domains take part in the interconnected or even co-continuous organizations. As reported, loading silica nanoparticles into PLA/P[CL-*co*-LA] blends leads to the increase in viscosity of the resulting compositions, retarding the coalescence of P[CL-*co*-LA] droplets and therefore affecting the overall shape and average size of dispersed microdomains (as proposed in Scheme 1). Similar results were reported by e.g. Ahn and Paul,[48] showing that the addition of clay into rubber-toughened Nylon-6 affected the dispersion of the rubber phase resulting in larger and elongated rubber microdomains. Co-continuous structures were even reported by several authors as a result of enhanced compatibility upon the addition of nanoadditives within immiscible polymer blends.[49–51] Accordingly, thermodynamic and kinetic driving forces are involved by enhancing the compatibility of PLA/P[CL-*co*-LA] blends depending on the specific localization of silica nanoparticles at their interface and by playing on the breakup/coalescence equilibrium, respectively. Importantly, such peculiar morphologies and the as-induced high toughness were fully preserved after reshaping/remolding the blends, giving similar values of the impact strength and confirming the stability of the observed structures.

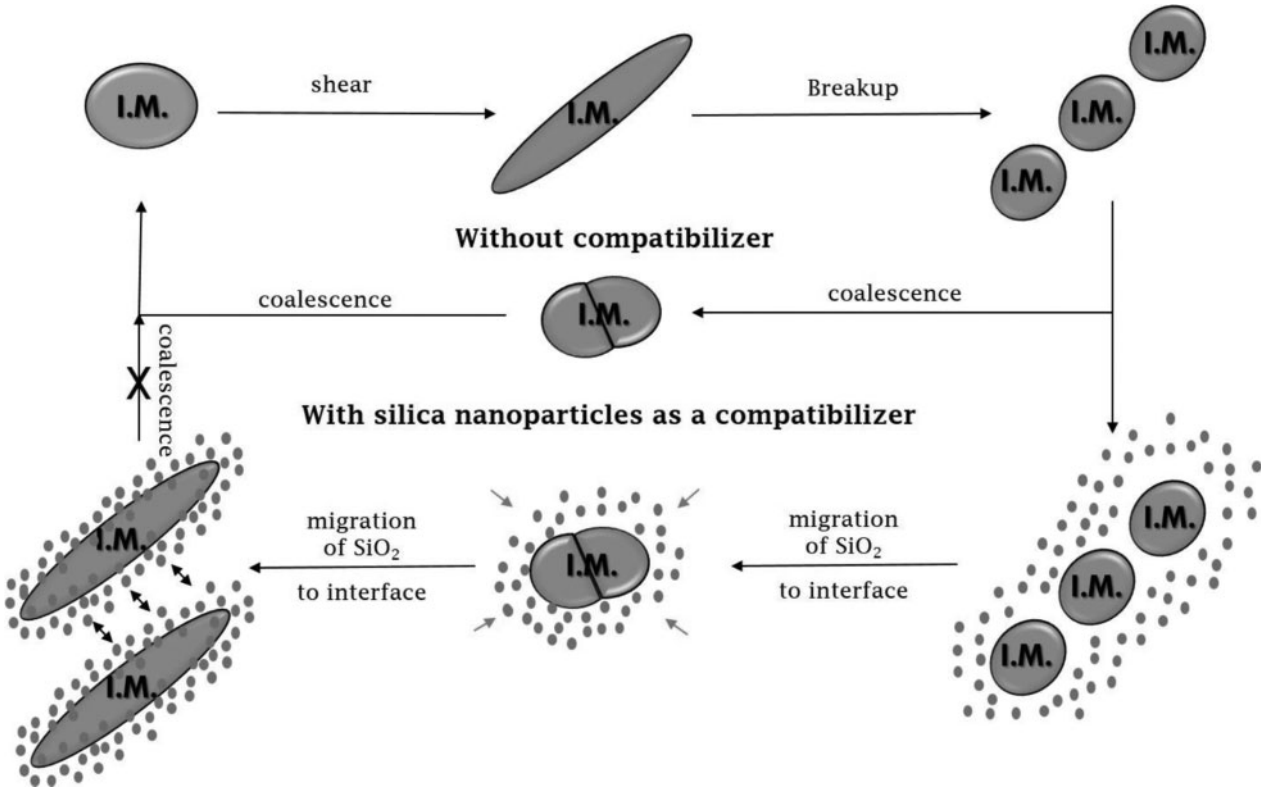

Scheme 1 Representation of the morphology evolution in immiscible PLA/P[CL-*co*-LA] blends compatibilized by silica nanoparticles

From the literature, rubber-toughening of polymers is extensively described based on toughening and fracture mechanisms, as called crazing, shear yielding, cavitation or debonding.[52–56] In this respect, Stoclet *et al.*[57] characterized the complex plastic deformation behavior exhibited by PLA, considering both the elementary mechanisms and the drawing kinetics. As expected, the crazing mechanism is responsible for the brittle character of PLA. In contrast, rubber-modified PLA can undergo one or a combination of the most dissipative toughening mechanisms. This owes to the classical role of the dispersed rubbery phase acting as local stress concentrators at many sites throughout the material and initiating greater energy dissipative micromechanisms. Indeed, starting from its optimum microdomain average size around 0.9 μm, it might result that internal cavitation of rubber droplets (needing droplets of size higher than 200 nm) is easily achieved within the rubber-toughened PLA/P[CL-*co*-LA] binary blend.[58,59] This releases the hydrostatic strain energy and involves, to some extent, the dissipation of energy and emergence of other energy absorbing mechanisms for the main matrix, e.g. craze initiation (at such relatively high microdomain size, higher than 0.5 μm). The emergence of such energy dissipative micromechanisms initiated by the rubbery microdomains is further highlighted in Fig. 7. As aforementioned, the occurrence of crazing (and/or cavitation and fibrillation) might be considered as the prevailing toughening mechanism within these PLA-based materials. The contribution of the latter increases upon the morphological change (from droplets to ribbons and finally to interconnected and even co-continuous structures) as induced by the presence of nanosilica at the PLA/P[CL-*co*-LA] interface. This suggests us that craze initiation occurs at a low stress level from these peculiar morphologies. The high volume of cavitated matter and the capacity of the continuous rubber phase to stabilize the damaged microstructure allow achieving high energy dissipation. In this respect, the authors may postulate that the high capacity for energy dissipation is related to the interconnection of such peculiar microstructures, which promotes extensive plasticity in thinner matrix ligaments, as compared to the previous binary blends. As a result, the contribution of dilatational toughening mechanisms increases with nanosilica content, enhancing the improved energy dissipation on impact stress conditions as another consequence (Fig. 7, middle). Besides craze growth, shear band nucleation further appears at an early stage in the presence of nanosilica, strengthening the ability of these materials to dissipate more energy before fracture (Fig. 7, bottom). It may be considered that the localization of silica nanoparticles at the PLA/P[CL-*co*-LA] interface strengthens the adhesion between polymer components, promoting interfacial cavitation under stress and releasing the triaxial state of stress. This therefore promotes shear band nucleation. Moreover, cavitational behavior became effective upon increasing deformation. Accordingly, this phenomenon favors the capacity of shear bands to stabilize craze growth, leading to improved energy dissipation before rupture. Even if the occurrence of shear banding is less pronounced than their cavitational counterpart, the combination of such energy dissipative micromechanisms leads to highly localized plastic deformation, endowing ultra-toughness of resulting materials. Scanning electron microscopy analysis along the draw axis on deformed samples confirms the presence of these specific deformations (Scheme 2). In the case of PLA/P[CL-*co*-LA] blends, macroscopic localized zones of micro-voids and micro-fibrils are observed after addition of a rubbery P[CL-*co*-LA] impact modifier within the PLA matrix and are related to crazing process on deformation. Further loading nanosilica within this PLA/P[CL-*co*-LA]-based blends imparted great ductility and impact strength to the materials, highlighting the uneven morphology change (from large droplets to small and long ribbons) and the formation of `infinite' self-networked (and even co-continuous) structures mediated by silica nanoparticles as a more effective way to toughen glassy materials. These features therefore support the statement that higher stress levels are required from these peculiar structures to generate cavitation and crazes in these materials, involving a combination of shear yielding and multiple crazing mechanisms.

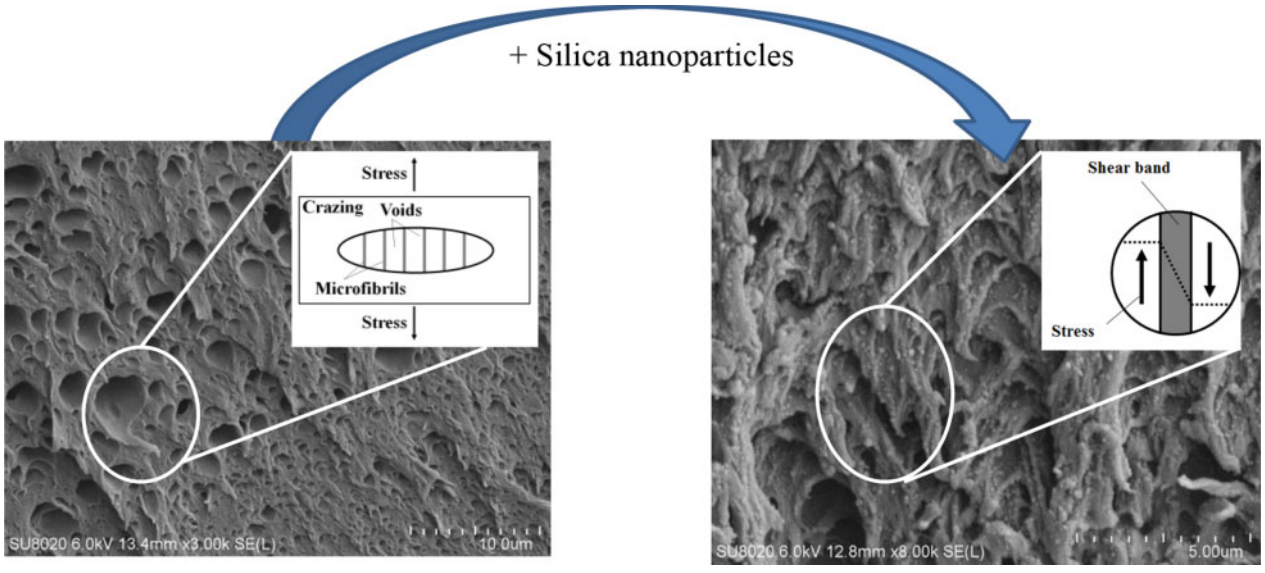

Scheme 2 Representation of brittle-to-ductile transition of immiscible PLA/P[CL-*co*-LA] blends after addition of silica nanoparticles

Conclusions

The compatibility of PLA/P[CL-*co*-LA] blends can be dramatically improved by the addition of silica nanoparticles, leading to the formation of self-networked (and even co-continuous) structures originated from rubbery impact modifier within the matrix. It was found that silica nanoparticles were mostly located at the PLA/P[CL-*co*-LA] interface, strengthening the interface of these peculiar morphologies. Using appropriate processing method and adjusting the affinity of silica nanoparticles through surface treatment, surface area and silica content, the conversion of rubbery spherical cavities into e.g. oblong structures in the presence of silica nanoparticles can be successfully reached, promoting, to some extent, filler-networks at 10 wt-% of TS-530, 5 wt-% of M-5 and 3 wt-% of H-5. The compatibilization mechanism of silica nanoparticles in PLA/P[CL-*co*-LA] blends and the progression to the uneven morphology change were proposed based on the coalescence and coarsening process. As reported, loading silica nanoparticles within PLA/P[CL-*co*-LA] blends leads to the increase in viscosity of resulting blends, impeding the coalescence of P[CL-*co*-LA] droplets while the migration and the nanosilica self-networking among the P[CL-*co*-LA] domains take part in the interconnected or even co-continuous organizations. Surprisingly, the co-addition of a P[CL-*co*-LA] rubbery impact modifier and silica nanoparticles in PLA through a two-step process increased significantly the material toughness as attested by the 18-fold increase recorded in impact strength with optimum stiffness/toughness balance. Accordingly, the resulting `infinite' network made of elongated rubbery domains mediated by the presence of silica nanoparticles affords a more efficient toughening strategy as compared to the individually dispersed spherical inclusions, which are often encountered in immiscible polymer blends. From these peculiar structures, it might result that a combination of shear yielding and multiple cavitational mechanisms provided large-scale deformation and high energy dissipation, determining the final mechanical performances of the as-produced PLA-based materials.

Conflicts of interest

The authors have no conflicts of interest to declare.

Acknowledgements

This research has been funded by the European Commission and Région Wallonne FEDER program in the frame of `Pôle d'Excellence Materia Nova' and OPTI$^2$MAT program of excellence, by the Interuniversity Attraction Poles program initiated by the Belgian Federal Science Policy Office (PAI 6/27 and P7/05) and by FNRS-FRFC. J. Odent thanks F.R.I.A. for its financial support thesis grant. J.-M. Raquez is `chercheur qualifié' by the F.R.S.-FNRS. Jean-Michel Thomassin is a `Logistics collaborator' by the F.R.S.-FNRS. Franck Lauro and Jean-Michel Gloaguen are `Professeur des Universités' at UVHC and Université Lille1, respectively.

References

1. Z. H. Liu, X. D. Zhang, X. G. Zhu, Z. N. Qi, F. S. Wang, R. K. Y. Li and C. L. Choy: *Polymer*, 1998, **39**, (21), 5047–5052.
2. S. Wu: *Polym. Eng. Sci.*, 1990, **30**, (13), 753–761.
3. K. Cho, J. Yang, S. Yoon, M. Hwang and S. V. Nair: *J. Appl. Polym. Sci.*, 2005, **95**, (3), 748–755.
4. Y. Okamoto, H. Miyagi, M. Kakugo and K. Takahashi: *Macromolecules*, 1991, **24**, (20), 5639–5644.
5. J. Odent, J. -M. Raquez, E. Duquesne and P. Dubois: *Eur. Polym. J.*, 2012, **48**, (2), 331–340.
6. A. K. Vegt and J. J. Elmendorp: 'Blending of incompatible polymers', in 'Integration of fundamental polymer science and technology' (ed. L. A. Kleintjens, et al.), 381–389; 1986, Netherlands, Springer.
7. C. Koning, M. Van Duin, C. Pagnoulle and R. Jerome: *Prog. Polym. Sci.*, 1998, **23**, (4), 707–757.
8. G. Wildes, H. Keskkula and D. R. Paul: *Polymer*, 1999, **40**, (20), 5609–5621.
9. I. Fortelný: *Eur. Polym. J.*, 2004, **40**, (9), 2161–2166.
10. S. Lyu, T. D. Jones, F. S. Bates and C. W. Macosko: *Macromolecules*, 2002, **35**, (20), 7845–7855.
11. A. E. Nesterov and Y. S. Lipatov: *Polymer*, 1999, **40**, (5), 1347–1349.
12. M. L. Di Lorenzo and M. Frigione: 'Compatibilization criteria and procedures for binary blends: a review'; 1997, Tel Aviv, Israel, Freund.
13. J. K. Kim, S. Kim and C. E. Park: *Polymer*, 1997, **38**, (9), 2155–2164.
14. M. F. Díaz, S. E. Barbosa and N. J. Capiati: *Polymer*, 2005, **46**, (16), 6096–6101.
15. B. B. Khatua, D. J. Lee, H. Y. Kim and J. K. Kim: *Macromolecules*, 2004, **37**, (7), 2454–2459.
16. L. Ashabi, S. H. Jafari, B. Baghaei, H. A. Khonakdar, P. Pötschke and F. Böhme: *Polymer*, 2008, **49**, (8), 2119–2126.
17. X. -Q. Liu, W. Yang, B. -H. Xie and M. -B. Yang: *Mater. Des.*, 2012, **34**, (0), 355–362.
18. M. Y. Gelfer, H. H. Song, L. Liu, B. S. Hsiao, B. Chu, M. Rafailovich, M. Si, V. Zaitsev and J. Polym: *J. Polym. Sci. B Polym. Phys.*, 2003, **41**, (1), 44–54.
19. H. Yang, X. Zhang, C. Qu, B. Li, L. Zhang, Q. Zhang and Q. Fu: *Polymer*, 2007, **48**, (3), 860–869.
20. I. Kelnar, J. Rotrekl, J. Kotek, L. Kaprálková and J. Hromádková: *Eur. Polym. J.*, 2009, **45**, (10), 2760–2766.
21. H. -S. Lee, P. D. Fasulo, W. R. Rodgers and D. R. Paul: *Polymer*, 2005, **46**, (25), 11673–11689.
22. E. Moghbelli, H. -J. Sue and S. Jain: *Polymer*, 2010, **51**, (18), 4231–4237.
23. W. Wu and Z. D. Xu: *Acta Pharmacol. Sin.*, 2000, **1**, 99–104.
24. S. Xinqing, Q. Jinliang, H. Youqing, L. Yiqun, Z. Xiaohong, G. Jianming, T. Banghui and S. Zhihai: *Acta Polymerica Sinica.*, 2005, **1**, 142–148.
25. C. G. Ma, Y. L. Mai, M. Z. Rong, W. H. Ruan and M. Q. Zhang: *Compos. Sci. Technol.*, 2007, **67**, (14), 2997–3005.
26. P. R. Hornsby and K. Premphet: *J. Appl. Polym. Sci.*, 1998, **70**, (3), 587–597.
27. F. Sahnoune, J. M. Lopez Cuesta and A. Crespy: *Polym. Eng. Sci.*, 2003, **43**, (3), 647–660.
28. S. Chang, T. Xie and G. Yang: *J. Appl. Polym. Sci.*, 2006, **102**, (6), 5184–5190.
29. H. Yang, Q. Zhang, M. Guo, C. Wang, R. Du and Q. Fu: *Polymer*, 2006, **47**, (6), 2106–2115.
30. J. Jancar and A. T. Dibenedetto: *J. Mater. Sci.*, 1994, **29**, (17), 4651–4658.
31. Y. Long and R. A. Shanks: *J. Appl. Polym. Sci.*, 1996, **61**, (11), 1877–1885.
32. Y. S. Lipatov: *Prog. Polym. Sci.*, 2002, **27**, (9), 1721–1801.
33. A. E. Nesterov, Y. S. Lipatov and T. D. Ignatova: *Eur. Polym. J.*, 2001, **37**, (2), 281–285.
34. Y. S. Lipatov, A. E. Nesterov, T. D. Ignatova and D. A. Nesterov: *Polymer*, 2002, **43**, (3), 875–880.
35. K. Madhavan Nampoothiri, N. R. Nair and R. P. John: *Bioresour. Technol.*, 2010, **101**, (22), 8493–8501.
36. R. Auras, B. Harte and S. Selke: *Macromol. Biosci.*, 2004, **4**, (9), 835–864.
37. K. S. Anderson, K. M. Schreck and M. A. Hillmyer: *Polym. Rev.*, 2008, **48**, (1), 85–108.
38. S. Ishida, R. Nagasaki, K. Chino, T. Dong and Y. Inoue: *J. Appl. Polym. Sci.*, 2009, **113**, (1), 558–566.
39. J. Odent, P. Leclère, J. -M. Raquez and P. Dubois: *Eur. Polym. J.*, 2013, **49**, (4), 914–922.
40. J. Odent, Y. Habibi, J. -M. Raquez and P. Dubois: *Compos. Sci. Technol.*, 2013, **84**, (0), 86–91.
41. F. Gubbels, S. Blacher, E. Vanlathem, R. Jerome, R. Deltour, F. Brouers and P. Teyssie: *Macromolecules*, 1995, **28**, (5), 1559–1566.
42. C. B. Bucknall and D. Clayton: *J. Mater. Sci.*, 1972, **7**, (2), 202–210.
43. S. I. Naqui and I. M. Robinson: *J. Mater. Sci.*, 1993, **28**, (6), 1421–1429.
44. P. François, J. M. Gloaguen, B. Hue and J. M. Lefebvre: *J. Phys. III France*, 1994, **4**, (2), 321–329.

Maney Publishing

45. C. G'Sell, J. M. Hiver and A. Dahoun: *Int. J. Solids Struct.*, 2002, **39**, (13–14), 3857–3872.
46. A. C. Renouf-Glauser, J. Rose, D. F. Farrar and R. E. Cameron: *Biomaterials*, 2005, **26**, (29), 5771–5782.
47. Q. Zhang, H. Yang and Q. Fu: *Polymer*, 2004, **45**, (6), 1913–1922.
48. Y. -C. Ahn and D. R. Paul: *Polymer*, 2006, **47**, (8), 2830–2838.
49. Y. Li and H. Shimizu: *Polymer*, 2004, **45**, (22), 7381–7388.
50. F. Gubbels, R. Jerome, P. Teyssie, E. Vanlathem, R. Deltour, A. Calderone, V. Parente and J. L. Bredas: *Macromolecules*, 1994, **27**, (7), 1972–1974.
51. Y. -H. Wang, Y. -Y. Shi, J. Dai, J. -H. Yang, T. Huang, N. Zhang, Y. Peng and Y. Wang: *Polym. Int.*, 2013, **62**, (6), 957–965.
52. W. G. Perkins: *Polym. Eng. Sci.*, 1999, **39**, (12), 2445–2460.
53. R. M. Ikeda: *J. Appl. Polym. Sci.*, 1993, **47**, (4), 619–629.
54. P. A. O'Connell and G. B. McKenna: 'Yield and crazing in polymers', in 'Encyclopedia of polymer science and technology'; (ed Herman F. Mark); 627–681; 2002, New York, John Wiley & Sons, Inc.
55. I. Narisawa and A. Yee: 'Crazing and fracture of polymers', in 'Materials science and technology'; (ed. Edwin L. Thomas), 698–765; 2006, Weinheim, Wiley-VCH Verlag GmbH & Co. KGaA.
56. D. K. Mahajan and A. Hartmaier: *Phys. Rev. E*, 2012, **86**, (2), 021802.
57. G. Stoclet, J. M. Lefebvre, R. Séguéla and C. Vanmansart: *Polymer*, 2014, **55**, (7), 1817–1828.
58. A. M. Donald and E. J. Kramer: *J. Appl. Polym. Sci.*, 1982, **27**, (10), 3729–3741.
59. D. Dompas, G. Groeninckx, M. Isogawa, T. Hasegawa and M. Kadokura: *Polymer*, 1994, **35**, (22), 4750–4759.